Optics Letters

Optomechanical response with nanometer resolution in the self-mixing signal of a terahertz quantum cascade laser

Andrea Ottomaniello,[1,2,*] James Keeley,[3] Pierluigi Rubino,[3] Lianhe Li,[3] Marco Cecchini,[2] Edmund H. Linfield,[3] A. Giles Davies,[3] Paul Dean,[3] Alessandro Pitanti,[2] and Alessandro Tredicucci[1,2]

[1]Dipartimento di Fisica "E. Fermi," Università degli studi di Pisa, 561217 Pisa, Italy
[2]NEST, CNR -Istituto Nanoscienze and Scuola Normale Superiore, Piazza San Silvestro 12, 56127 Pisa, Italy
[3]School of Electronic and Electrical Engineering, University of Leeds, Leeds LS29JT, UK
*Corresponding author: andrea.ottomaniello@df.unipi.it

Received 13 August 2019; accepted 2 October 2019; posted 8 October 2019 (Doc. ID 374949); published 20 November 2019

Owing to their intrinsic stability against optical feedback (OF), quantum cascade lasers (QCLs) represent a uniquely versatile source to further improve self-mixing interferometry at mid-infrared and terahertz (THz) frequencies. Here, we show the feasibility of detecting with nanometer precision, the deeply subwavelength ($< \lambda/6000$) mechanical vibrations of a suspended Si_3N_4 membrane used as the external element of a THz QCL feedback interferometer. Besides representing an extension of the applicability of vibrometric characterization at THz frequencies, our system can be exploited for the realization of optomechanical applications, such as dynamical switching between different OF regimes and a still-lacking THz master-slave configuration.

Published by The Optical Society under the terms of the Creative Commons Attribution 4.0 License. Further distribution of this work must maintain attribution to the author(s) and the published article's title, journal citation, and DOI.

https://doi.org/10.1364/OL.44.005663

The self-mixing (SM) effect describes the interference of the intracavity electromagnetic field of a laser with its emitted radiation partially reinjected into the laser cavity [1]. Although such optical feedback (OF) can be detrimental to laser operation [2], the SM effect can also be exploited for metrological applications [3] through a technique known as laser-feedback interferometry (LFI) [4]. This homodyne technique, in which the laser acts simultaneously as source, mixer, and shot-noise limited detector, allows the retrieval of information about the external cavity, composed of the target and the external medium, by monitoring the response of the laser to OF. Thanks to the universal character of the SM phenomenon, its functionality has been demonstrated from the visible to the microwave range using laser systems as diverse as gas lasers [3], solid-state lasers [5], and semiconductor lasers [6]. This has led to the development of a large number of sensing applications [7] ranging from displacement measurement [8] to material analysis [9], laser emission spectrometry [10], and coherent imaging [11,12]. Among all kinds of semiconductor lasers, quantum cascade lasers (QCLs) allow further simplification of the SM scheme, thanks to their intrinsic voltage sensitivity to OF. This allows the SM modulation to be measured directly and with high sensitivity [13] via the voltage variation across the active region with no need for an external photodetector [14]. Moreover, QCLs exhibit peculiar ultra-stability to OF [15] due to their small linewidth enhancement factor [16] ($0 < |\alpha| < 1$) and long photon-to-carrier lifetime ratio. These unique and versatile characteristics offer an opportunity for the development of high-performance LFI schemes operating at mid-infrared and terahertz (THz) frequencies for coherent imaging [17] and displacement sensing [18,19]. In fact, despite the relatively long wavelength, nanometer target displacements as low as $\lambda/100$ have been measured by adding a fast-moving etalon in the external cavity [20] and 60–70 nm in-plane spatial resolution with both amplitude and phase contrast through THz scattering-type scanning near-field optical microscopy [21].

In this Letter, we report a significant improvement of nanometer displacement sensing by showing the detection of deeply subwavelength vibrations ($< \lambda/6000$) of a suspended mechanical resonator by employing a 3.34 THz QCL operating in continuous-wave (CW). The experimental results have been validated by solving the Lang–Kobayashi (LK) model [22] in the steady-state regime after calibration of the absolute membrane position. Furthermore, the measured oscillation amplitudes are shown to be in agreement with independent measurements performed using a laser Doppler vibrometer (LDV) operating in the visible region.

We chose as an external element a Si_3N_4 trampoline membrane, which is an optimum candidate for interferometric readout and optomechanical applications [23]. Such membranes have already been used to observe optomechanical features in an infrared laser diode SM configuration [24]. A scanning electron microscope (SEM) image of the fabricated sample is shown in Fig. 1(a). The structure is composed of a

300 nm thick, 300 μm wide suspended central pad held at each corner by 10 μm wide tethers anchored at the vertices of a 1 mm side square window. The details of the sample fabrication can be found elsewhere [24]. The membrane pad dimensions were chosen in order to increase the level of OF for SM measurements by creating a reflective surface of size comparable to the focused THz beam spot size (∼ 250 μm). To further increase the reflectivity, a 10 nm thick gold layer was thermally evaporated over the entire membrane surface to produce an almost totally reflective target. The sample was directly glued on the top surface of a piezoelectric ceramic actuator with the fundamental out-of-plane mechanical resonance at ∼ 100 kHz. The system composed of the piezo-actuator and membrane sample was mounted inside a vacuum chamber allowing control of the environmental pressure. An initial membrane characterization was performed using a commercial high-spatial-resolution LDV (Polytech UHF 120).

From the spectrum shown in Fig. 1(b), obtained at atmospheric pressure by applying a flat spectrum voltage excitation to the piezo-actuator, the fundamental mechanical mode (highlighted in the inset) is observed to be well separated from the higher-order modes. Moreover, with the membrane oscillating orthogonally to the chip-plane, this particular mode ensures that the full THz wavefront reflected from the membrane experiences the same external optical path. This makes the fundamental vibrational mode particularly suitable for coherent measurements of membrane vibrations by LFI [24] and, as such, subsequent measurements here focus on this mode. A LDV characterization of the membrane fundamental mode as a function of pressure was performed. The data were analyzed by modelling the membrane as a one-dimensional driven harmonic oscillator. Defining $A(t)$ and $a(t)$ as the positions of the membrane trampoline and of the tether clamps with respect to their common rest positions $A = a = 0$, respectively, the membrane equation of motion can be written as

$$\ddot{A}(t) + \gamma \dot{A}(t) + \omega_m^2 [A(t) - a(t)] = 0, \tag{1}$$

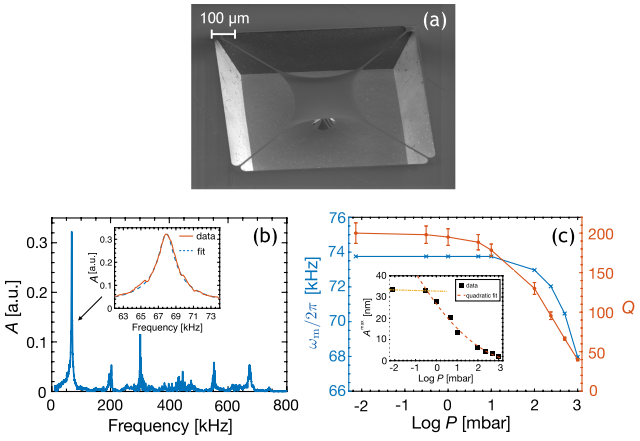

Fig. 1. (a) SEM image of the Si_3N_4 membrane. (b) Membrane mechanical spectrum measured at atmospheric pressure at the membrane center using the LDV. Inset: zoom of the fundamental resonance and corresponding fit (dashed line) using Eq. (2). (c) $\omega_m/2\pi$, Q, and A^{max} as a function of P in logarithmic scale. The dashed curve is a quadratic fit for the data down to $P = 1$ mbar, while the dashed line indicates the saturation effect observed below this pressure.

where ω_m is the pressure-dependent membrane resonance angular frequency, and γ is the membrane damping coefficient. The oscillation amplitude can be obtained from the imaginary part of the solution, $A(\omega)$, in the frequency domain:

$$\mathrm{Im}[A(\omega)] = \frac{\gamma\omega}{(\omega_m^2 - \omega^2)^2 + (\gamma\omega)^2}\omega_m^2 a_0, \tag{2}$$

where $a_0 \sim 60 \pm 2$ pm is the maximum driving oscillation amplitude.

By fitting the displacement spectra using Eq. (2), we obtain for each investigated pressure the values of the resonance frequency $\omega_m/2\pi$, the quality factor $Q = \omega_m/\gamma$, and the oscillation amplitude at the resonance frequency A^{max}. As the environmental pressure decreases, these three quantities monotonically increase up to a saturation level [see Fig. 1(c)]. The resonance frequency and quality factor change from $\omega_m/2\pi \sim 67.9$ kHz and $Q \sim 40 \pm 2$, respectively, at atmospheric pressure to ~ 73.4 kHz and $\sim 200 \pm 10$ at pressure $P \sim 7.3 \times 10^{-3}$ mbar.

A schematic diagram of the experimental apparatus for the THz LFI measurements is presented in Fig. 2(a). We used a THz QCL consisting of a 14 μm thick GaAs-AlGaAs active region with growth details reported in the literature [25]. The device was fabricated as a single-metal ridge with longitudinal and transversal dimensions of 1.8 mm and 150 μm, respectively. The laser was driven in the CW mode with a current equal to 510 mA and was maintained at a temperature of 25 K using a continuous-flow cryostat. Under these conditions, the QCL provided stable single-mode emission at 3.34 THz and a large SM response [13,25]. The THz beam passing through the polythene window of the cryostat was collimated and focused (using two $f/2$ off-axis parabolic reflectors with a diameter of 50.8 mm) onto the trampoline membrane which constituted the mirror of the external cavity. The vacuum chamber containing the membrane was fixed to a motorized stage allowing the external optical cavity length L between the target and the QCL emission facet to be micrometrically changed. The LFI apparatus was used in two configurations. In the first configuration [conf. 1 in Fig. 2(a)], the membrane motion was not excited, and the membrane was moved towards the laser facet in 2 μm long steps parallel to the beam propagation direction. The QCL SM voltage V_{SM} was measured by a lock-in amplifier synchronized to the optical modulation frequency ($\nu_{mod} = 212$ Hz) imposed to the THz beam by a mechanical chopper placed in front of the vacuum chamber. In the second configuration [conf. 2 in Fig. 2(a)], the membrane equilibrium position instead was kept fixed, but the membrane vibrated at the frequency of the piezo driving excitation which, in turn, was used as the reference of the lock-in amplifier.

To model the SM voltage signal as a function of the target position, we used the steady-state solutions of the LK equations describing the laser under OF [22]. This was done by evaluating the laser emission frequency under OF, ω_F, by numerically solving the so-called excess phase equation:

$$\omega_0 - \omega_F = \frac{k}{\tau_c}\sqrt{1+\alpha^2}\,\sin(\omega_F \tau_{ext} + \arctan\alpha), \tag{3}$$

where ω_0 is the laser emission frequency without feedback, τ_c is the laser cavity round-trip time, $\tau_{ext} = 2L/c$ is the round-trip time in the external cavity, α is Henry's linewidth enhancement

factor, and k is the OF coupling rate. Using the conventional three-mirror model in the weak feedback regime, where only one reflection from the target is considered, k can be written as $k = \epsilon\sqrt{\frac{R_{\text{ext}}}{R}}(1-R)$, in which ϵ, R, and R_{ext} are the coupling-efficiency factor and the reflectivities of the target and laser emission facet, respectively. The parameter ω_{F} obtained from Eq. (3) determines the laser carrier number variation ΔN from the threshold carrier number with and without feedback via the following equation:

$$\Delta N = -\frac{2k}{G\tau_c}\cos(\omega_{\text{F}}\tau_{\text{ext}}), \tag{4}$$

where G is the modal gain factor. Starting from the initial external cavity optical length, $L_0 = 47$ cm, ΔN was calculated for each value of L using the following best fitting parameters: $\tau_c = 43.8$ ps, $k = 1.28 \times 10^{-2}$, $\alpha = 0.5$, and $G = 1.42 \times 10^4$ s^{-1}. The values of ΔN are plotted (blue curve) as a function of the membrane displacement $\Delta L = L_0 - L$ in Fig. 2(b), together with the experimental values V_{SM} (red points) obtained with configuration 1. The theoretical values are in good agreement with the experiment reproducing both the same shape and typical periodicity ($\lambda_F/2$) of the SM signal. From a comparison of these curves, we obtained the proportionality coefficient β between the calculated ΔN and the measured V_{SM}, found to be 3.1×10^{-8} mV. It should be noted that the calibration factor β depends on the particular value of G, which was fixed according to common values in THz QCL literature [26,27]. Nevertheless, our calibration procedure allows us to correlate experiments and simulations independently of the value assigned to G.

SM measurements of the membrane oscillation amplitude were then performed using configuration 2. V_{SM} measured at

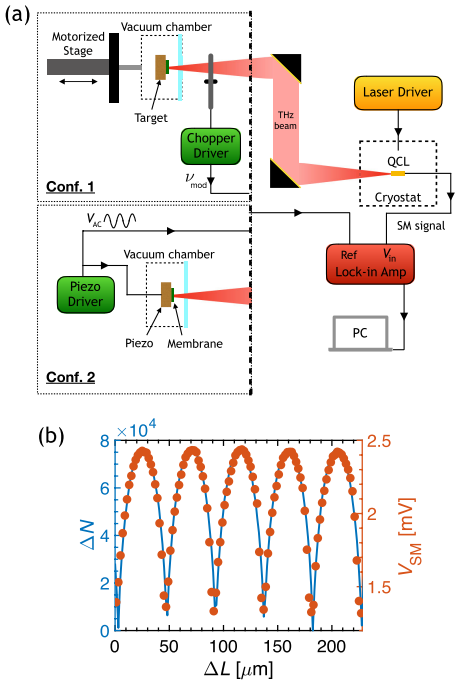

Fig. 2. (a) Sketch of the two configurations of the SM apparatus. (b) Calculated ΔN (blue curve), and measured V_{SM} (red points) as a function of ΔL using configuration 1.

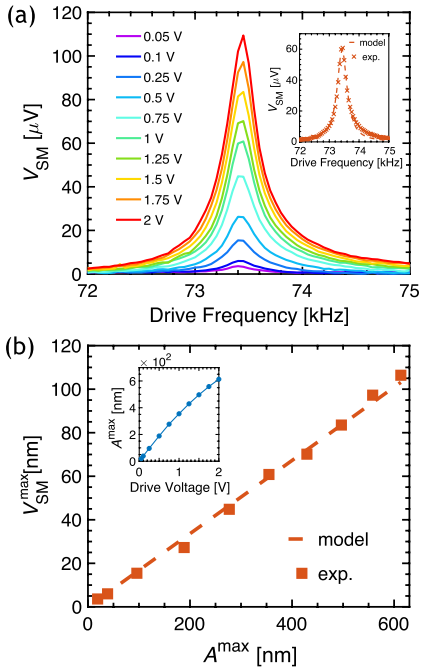

Fig. 3. (a) Measured V_{SM} as a function of the drive frequency for different applied voltages at $P = 0.5$ mbar. Inset: computed (red dashed line) and experimental (red crosses) V_{SM} spectrum with 1 V_{RMS} applied to the piezo-actuator. (b) Measured (red squares) and calculated (dashed line) $V_{\text{SM}}^{\text{max}}$ as a function of A^{max}. Inset: LDV-measured A^{max}.

an environmental pressure of $P = 0.5$ mbar is reported as a function of the drive frequency and for several RMS drive voltages in Fig. 3(a). Using a Lorentzian spectral line-shape as the fitting function for the data (valid in the experimentally verified high-Q limit), the vibration spectra were observed to have the same resonance frequency $\omega_{\text{m}}/2\pi \sim 73.43 \pm 0.01$ kHz and $Q \sim 198 \pm 2$, independent of the bias applied to the piezo-actuator. These quantities agree with those obtained previously with the LDV. The V_{SM} signal measured in response to the membrane vibrations can be modelled with Eqs. (3) and (4) for the steady-state solution of the LK model. In fact, with the limit $2\pi/\tau_{\text{ext}} \gg \omega_{\text{m}}$ satisfied, the membrane position at each instant in time can be considered fixed, contributing as a static external optical path for the LK equations. The time-dependent variation of carrier number $\Delta N(t)$ corresponding to a certain membrane oscillation amplitude can thus be numerically obtained by inserting into Eqs. (3)–(4) the following expression for L:

$$L = L_0 + A(\omega)\cos(\omega_{\text{m}} t), \tag{5}$$

where $A(\omega)$ is the drive frequency-dependent membrane oscillation amplitude [Eq. (2)] evaluated using the previously fitted values of γ and ω_{m}. The total carrier number variation corresponding to the membrane vibration at a given drive frequency, $\Delta N(\omega)$, can then be calculated as the peak-to-peak amplitude of the time-oscillating $\Delta N(t)$. V_{SM} can then be obtained just multiplying $\Delta N(\omega)$ by the previously retrieved β-factor. In the inset of Fig. 3(a), the values of V_{SM} resulting from this model are shown to reproduce well the experimental V_{SM} measured by applying a drive bias of 1 V_{RMS} spanning a single frequency

at a time in the range 72–75 kHz. For that drive voltage, both model and experimental result in a maximum SM signal of $\sim 61 \pm 1$ μV obtained for a $A = 355 \pm 5$ nm. Only a small deviation between the data and the model was found on the high-frequency side of the resonance, which we ascribe to a small degree of mechanical anharmonicity of the tethers' motion not being included in the model. Both the theoretical and experimental maximum SM voltages, $V_{\mathrm{SM}}^{\max}$, are shown in Fig. 3(b) as a function of the membrane maximum oscillation amplitude, $A^{\max}$. For the experimental points, the reported values of $A^{\max}$ are those obtained from the LDV measurements at the same piezo-actuator drive voltage as the SM measurements, and they are shown in the inset as a function of the applied bias. From the main graph, it can be observed that the model matches the experimental data and confirms a linear relation between $V_{\mathrm{SM}}^{\max}$ and $A^{\max}$ with a slope coefficient of 0.17 ± 0.01 μV/nm. This agreement implies that we are able to detect membrane vibrations with appreciable precision (≤ 10 nm, limited by the voltage noise of our setup) down to deeply subwavelength oscillation amplitudes of only a few nanometers. Specifically, the amplitude corresponding to a SM signal ≥ 3 dB above the voltage noise is $\sim 15 \pm 5$ nm. The high observed SM voltage sensitivity to displacement results from the high slope of the SM voltage between the top and the minimum of a fringe in the *static* SM signal [see Fig. 2(b)]. In fact, since we were considering displacements $A^{\max} \ll \lambda/2$, the SM voltage sensitivity is expected to be proportional to the derivative of the *static* SM signal. In our case, the observed sensitivity corresponds to a distance from the maximum *static* SM voltage of ~ 12 μm which, indeed, falls in the rapidly decreasing side of a fringe. Interestingly, a sensitivity up to $\sim 0.83 \pm 0.02$ μV/nm, in principle, can be achieved in our system by fixing the membrane equilibrium position as close as possible to the minimum of the static SM voltage (corresponding to the maximum slope). In conclusion, we have experimentally demonstrated the detection of deeply subwavelength vibrations ($< \lambda/6000$) by LFI in the THz frequency range and using as an external element a suspended Si_3N_4 membrane. The SM voltage signal arising across the THz QCL active region in response to nanometer oscillations of the membrane was reproduced and uniquely determined by numerically solving the LK model in the steady-state regime. Thus, our measurement extends the applicability of LFI at THz frequencies for the vibrometric characterization of a variety of systems, especially those presenting the optical response at these frequencies. The mechanical resonator in the LFI apparatus can also represent a mechanical switch between different feedback regimes. A two-state system thus can be realized by placing the membrane near the position where the crossing between the two regimes arises. Moreover, the proposed LFI system can be employed for optomechanical applications where the suspended membrane is driven by radiation pressure; the realization of an optomechanical system constituted by two different lasers coupled through the mechanical motion driven by radiation pressure represents a promising perspective for the realization of a still-lacking master-slave configuration at THz frequencies.

Funding. Engineering and Physical Sciences Research Council (EP/P021859/1); Royal Society; Wolfson Foundation; GRANT ATTRACT project (GA 777222) European Research Council (Advanced Grant No. 321122 SouLMan).

Acknowledgment. E. Linfield and A. Davies are grateful for the support from the Royal Society and Wolfson Foundation.

REFERENCES

1. D. M. Kane and K. A. Shore, *Unlocking Dynamical Diversity: Optical Feedback Effects on Semiconductor Lasers* (Wiley, 2005).
2. D. Kleinman and P. Kisliuk, Bell Syst. Tech. J. **41**, 453 (1962).
3. P. King and G. Steward, New Sci. **17**, 14 (1963).
4. T. Taimre, M. Nikolić, K. Bertling, Y. L. Lim, T. Bosch, and A. D. Rakić, Adv. Opt. Photonics **7**, 570 (2015).
5. P. Nerin, P. Puget, P. Besesty, and G. Chartier, Electron. Lett. **33**, 491 (1997).
6. A. Seko, Y. Mitsuhashi, T. Morikawa, J. Shimada, and K. Sakurai, Appl. Phys. Lett. **27**, 140 (1975).
7. G. Giuliani, M. Norgia, S. Donati, and T. Bosch, J. Opt. A **4**, S283 (2002).
8. S. Donati, G. Giuliani, and S. Merlo, IEEE J. Quantum Electron. **31**, 113 (1995).
9. A. D. Rakić, T. Taimre, K. Bertling, Y. L. Lim, P. Dean, D. Indjin, Z. Ikonić, P. Harrison, A. Valavanis, S. P. Khanna, and M. Lachab, Opt. Express **21**, 22194 (2013).
10. J. Keeley, J. Freeman, K. Bertling, Y. L. Lim, R. A. Mohandas, T. Taimre, L. H. Li, D. Indjin, A. D. Rakić, E. H. Linfield, and A. G. Davies, Sci. Rep. **7**, 7236 (2017).
11. P. Dean, A. Valavanis, J. Keeley, K. Bertling, Y. Leng Lim, R. Alhathlool, S. Chowdhury, T. Taimre, L. H. Li, D. Indjin, and S. J. Wilson, Appl. Phys. Lett. **103**, 181112 (2013).
12. M. Wienold, T. Hagelschuer, N. Rothbart, L. Schrottke, K. Biermann, H. Grahn, and H.-W. Hübers, Appl. Phys. Lett. **109**, 011102 (2016).
13. J. Keeley, K. Bertling, P. L. Rubino, Y. L. Lim, T. Taimre, X. Qi, I. Kundu, L. H. Li, D. Indjin, A. D. Rakić, E. H. Linfield, A. G. Davies, J. Cunningham, and P. Dean, Opt. Lett. **44**, 3314 (2019).
14. P. Dean, Y. L. Lim, A. Valavanis, R. Kliese, M. Nikolić, S. P. Khanna, M. Lachab, D. Indjin, Z. Ikonić, P. Harrison, and A. D. Rakić, Opt. Lett. **36**, 2587 (2011).
15. F. Mezzapesa, L. Columbo, M. Brambilla, M. Dabbicco, S. Borri, M. Vitiello, H. Beere, D. Ritchie, and G. Scamarcio, Opt. Express **21**, 13748 (2013).
16. R. P. Green, J.-H. Xu, L. Mahler, A. Tredicucci, F. Beltram, G. Giuliani, H. E. Beere, and D. A. Ritchie, Appl. Phys. Lett. **92**, 071106 (2008).
17. P. Dean, A. Valavanis, J. Keeley, K. Bertling, Y. Lim, R. Alhathlool, A. Burnett, L. Li, S. Khanna, D. Indjin, and T. Taimre, J. Phys. D **47**, 374008 (2014).
18. Y. Leng Lim, P. Dean, M. Nikolić, R. Kliese, S. P. Khanna, M. Lachab, A. Valavanis, D. Indjin, Z. Ikonić, P. Harrison, and E. H. Linfield, Appl. Phys. Lett. **99**, 081108 (2011).
19. F. Mezzapesa, L. Columbo, M. Dabbicco, M. Brambilla, and G. Scamarcio, Opt. Express **22**, 5867 (2014).
20. F. P. Mezzapesa, L. L. Columbo, G. De Risi, M. Brambilla, M. Dabbicco, V. Spagnolo, and G. Scamarcio, IEEE J. Sel. Top. Quantum Electron. **21**, 107 (2015).
21. M. C. Giordano, S. Mastel, C. Liewald, L. L. Columbo, M. Brambilla, L. Viti, A. Politano, K. Zhang, L. Li, A. G. Davies, E. H. Linfield, R. Hillenbrand, F. Keilmann, G. Scamarcio, and M. S. Vitiello, Opt. Express **26**, 18423 (2018).
22. R. Lang and K. Kobayashi, IEEE J. Quantum Electron. **16**, 347 (1980).
23. R. A. Norte, J. P. Moura, and S. Gröblacher, Phys. Rev. Lett. **116**, 147202 (2016).
24. L. Baldacci, A. Pitanti, L. Masini, A. Arcangeli, F. Colangelo, D. Navarro-Urrios, and A. Tredicucci, Sci. Rep. **6**, 31489 (2016).
25. M. Wienold, L. Schrottke, M. Giehler, R. Hey, W. Anders, and H. Grahn, Electron. Lett. **45**, 1030 (2009).
26. G. Agnew, A. Grier, T. Taimre, Y. L. Lim, K. Bertling, Z. Ikonić, A. Valavanis, P. Dean, J. Cooper, S. P. Khanna, and M. Lachab, Opt. Express **24**, 20554 (2016).
27. A. Hamadou, J.-L. Thobel, and S. Lamari, Opt. Commun. **281**, 5385 (2008).